Supporting Information

New Magic Au_{24} Cluster Stabilized by PVP: Selective Formation, Atomic Structure, and Oxidation Catalysis

Shingo Hasegawa,[1] Shinjiro Takano,[1] Koji Harano,[1] and Tatsuya Tsukuda*[1,2]

[1] *Department of Chemistry, Graduate School of Science, The University of Tokyo, 7-3-1 Hongo, Bunkyo-ku, Tokyo 113-0033, Japan.*

[2] *Elements Strategy Initiative for Catalysts and Batteries (ESICB), Kyoto University, Katsura, Kyoto 615-8520, Japan.*

Table S1. Structural Parameters Obtained by Curve-Fitting Analysis of Au L_3-Edge EXAFS

Sample	Bond	CN [a]	r / Å [b]	σ^2 / Å^2 [c]	R / % [d]
Au_{24}:PVP as synthesized (**Fig. 2c, Fig. S19: black**)	Au–Cl	0.7 ± 0.2	2.34 ± 0.02	0.007 ± 0.004	7.4
	Au–Au	4.2 ± 0.5	2.71 ± 0.01	0.0086 ± 0.0009	
Au_{24}:PVP after catalytic usage (**Fig. S19: red**)	Au–Au	4.7 ± 0.4	2.72 ± 0.01	0.0094 ± 0.0008	15.0

[a] Coordination number. [b] Bond length. [c] Debye-Waller factor.
[d] $R = (\sum (k^3\chi^{data}(k)-k^3\chi^{fit}(k))^2)^{1/2}/(\sum (k^3\chi^{data}(k))^2)^{1/2}$.

Table S2. Au–Au Coordination Numbers (CNs) and Average Au–Au Bond Lengths (<r>) of DFT-Optimized Au_{24} in Figure 3 and $Au_{24}Cl_4$ in Figure 4.

Au_{24}			$Au_{24}Cl_4$		
Structure	CN [a]	<r> / Å [a]	Structure	CN [a]	<r> / Å [a]
1	5.2	2.88	**1Cl**	4.8	2.86
2	5.0	2.88	**2Cl**	4.6	2.85
3	5.4	2.89	**3Cl**	4.3	2.86
4	5.3	2.87	**4Cl**	4.3	2.85
5	5.2	2.90	**5Cl**	4.3	2.87
6	5.3	2.88	**6Cl**	4.2	2.87
7	5.0	2.90			

[a] Pairs of Au atoms with an interatomic distance smaller than 3.05 Å were considered to be bonded.

Table S3. Adsorption Energies and Stretching Frequencies of CO at Different Sites of Structure 1.

Structure	E_{ads} / eV	v(CO) /cm^{-1}	Structure	E_{ads} / eV	v(CO) / cm^{-1}
1COa^0	0.32	2109	**1COa$^-$**	0.22	2066
1COb^0	0.28	2109	**1COb$^-$**	0.10	2020
1COc^0	0.27	2113	**1COc$^-$**	0.29	2065
1COd^0	0.23	2103	**1COd$^-$**	0.14	2032
1COe^0	0.23	2110	**1COe$^-$**	0.21	2070
1COf^0	0.17	2108	**1COf$^-$**	0.11	2073
1COg^0	0.13	2113	**1COg$^-$**	0.16	2067
1COh^0	0.11	2105	**1COh$^-$**	0.17	2068

Table S4. Adsorption Energies and Stretching Frequencies of CO at Different Sites of Structure 4.

Structure	E_{ads} / eV	v(CO) /cm^{-1}	Structure	E_{ads} / eV	v(CO) / cm^{-1}
4COa^0	0.42	2103	**4COa$^-$**	0.31	2066
4COb^0	0.23	2118	**4COb$^-$**	0.28	2066
4COc^0	0.19	2107	**4COc$^-$**	0.38	2059

Description of the Supplementary Movies

Movie S1: ACTEM video of a single particle (**#8**) of Au_{24}:PVP (*t*: 24.04 – 36.00 s from the beginning of the video recording). The frame rate (5 fps) is five times slower than the actual rate (25 fps).

Movie S2: ACTEM video of a single particle (**#8**) of Au_{24}:PVP (*t*: 60.04 – 72.00 s from the beginning of the video recording). The frame rate (5 fps) is five times slower than actual the rate (25 fps).

Movie S3: ACTEM video of a single particle (**#8**) of Au_{24}:PVP (*t*: 84.04 – 96.00 s from the beginning of the video recording). The frame rate (5 fps) is five times slower than the actual rate (25 fps).

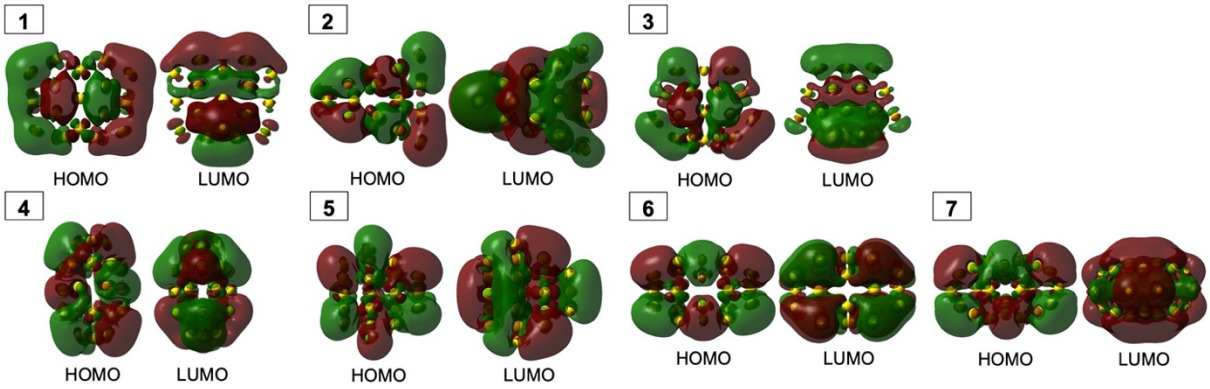

Figure S1. Frontier Kohn–Sham orbitals of model Au_{24} clusters shown in **Figure 3**.

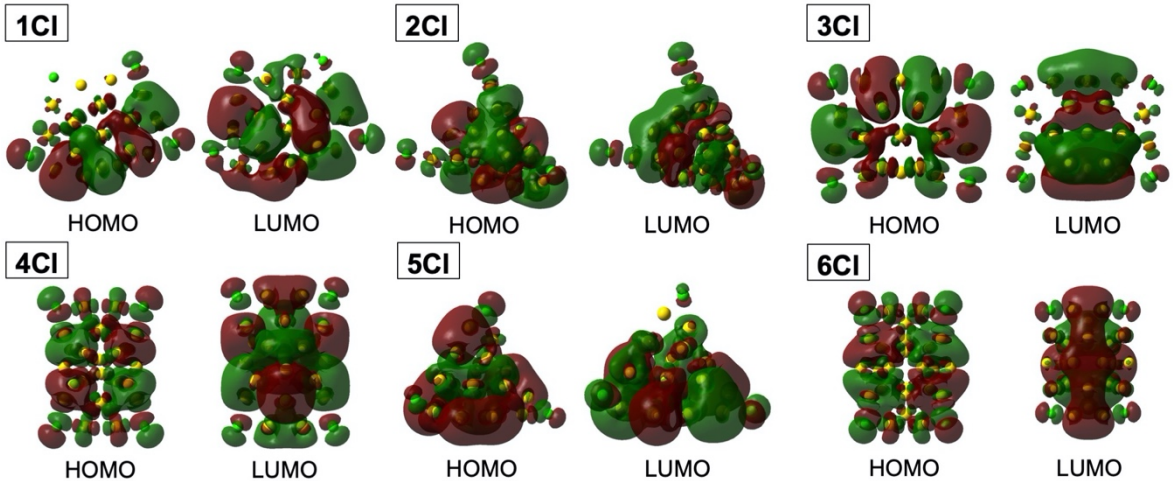

Figure S2. Frontier Kohn–Sham orbitals of model $Au_{24}Cl_4$ clusters shown in **Figure 4**.

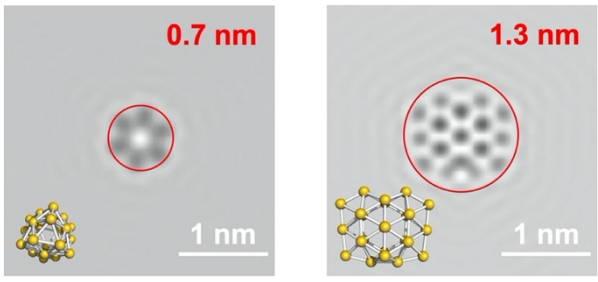

Figure S3. Simulated TEM images with (left) minimum (model **4**) and (right) maximum (model **1**) diameter.

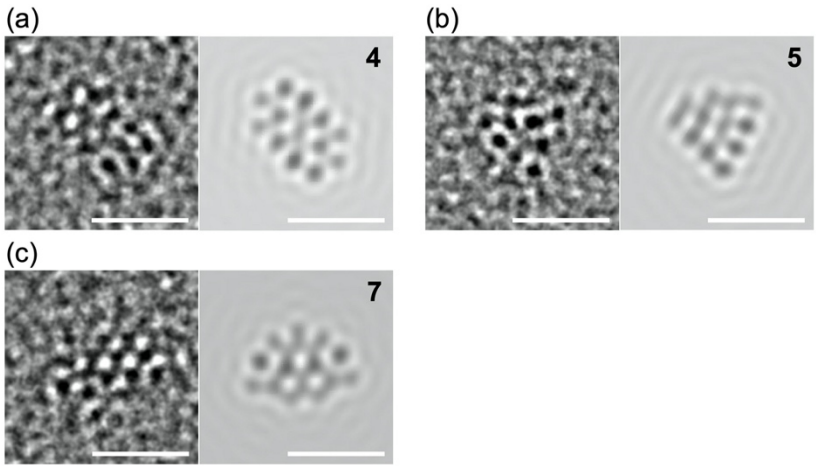

Figure S4. ACTEM images of different particles (**#5**–**#7**) of Au_{24}:PVP and simulated images of the model structures in **Figure 3**. The scale bars correspond to 1 nm.

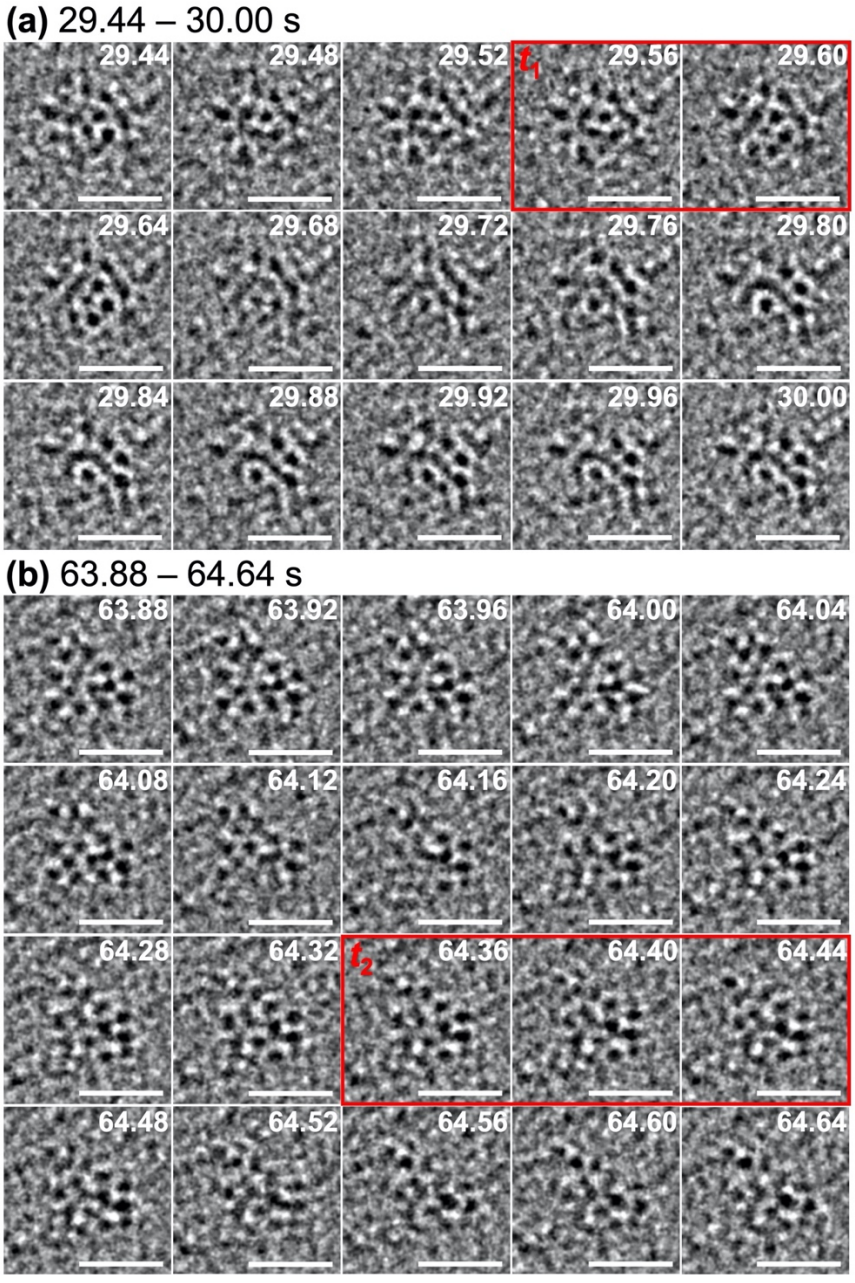

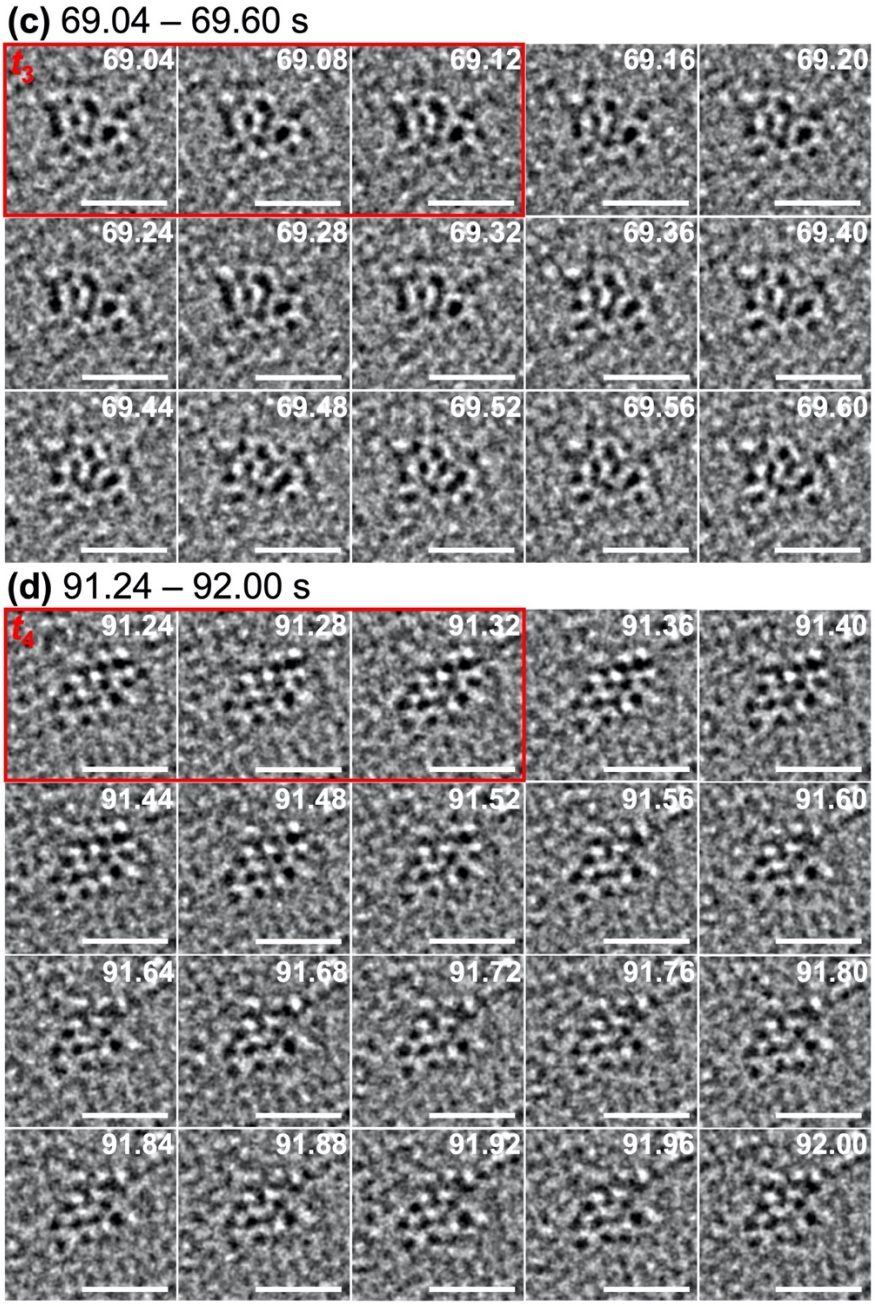

Figure S5. ACTEM image sequences of a single particle of Au_{24}:PVP (**#8**). The value in the upper right of each image shows the time in seconds from the beginning of the video recording. The scale bars correspond to 1 nm. The TEM images at t_1–t_4 in **Figure 6a** were obtained by averaging the images outlined by red lines in (a)–(d), respectively.

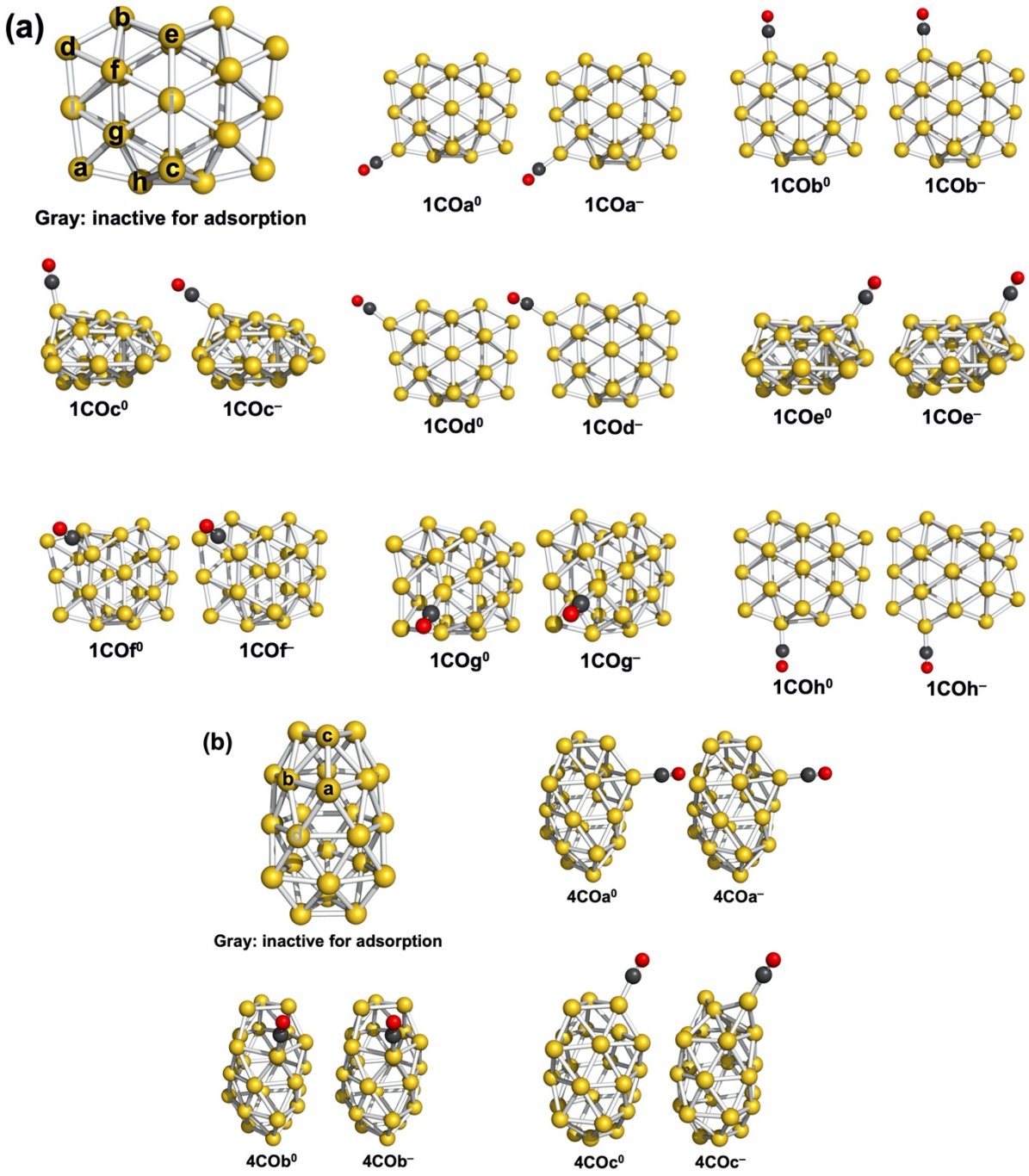

Figure S6. Adsorption sites and optimized structures for models (a) **1** and (b) **4**.

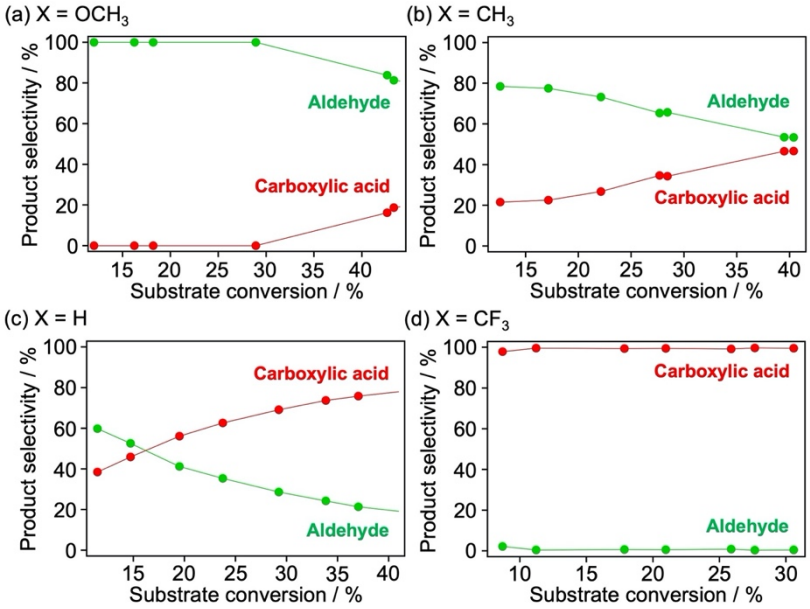

Figure S7. Product selectivity of the aerobic oxidation of *p*-substituted benzyl alcohol, X-$C_6H_4CH_2OH$ (X = OCH_3, CH_3, H, CF_3), shown in **Figure 8**.

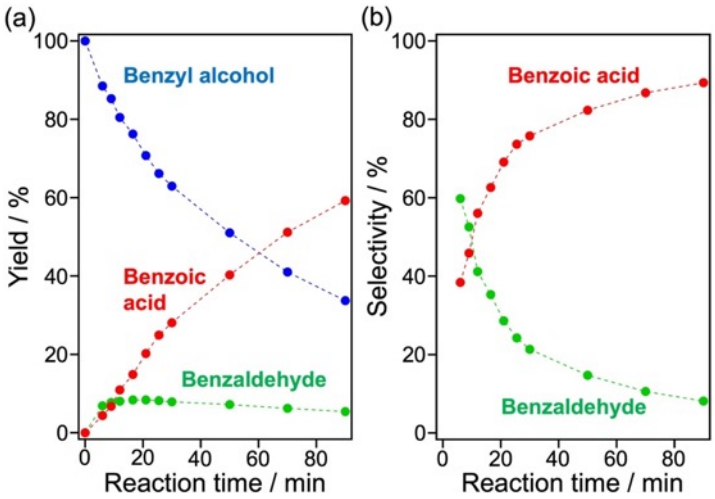

Figure S8. Time course of the (a) yield and (b) selectivity in the catalytic oxidation of benzyl alcohol at 303 K.

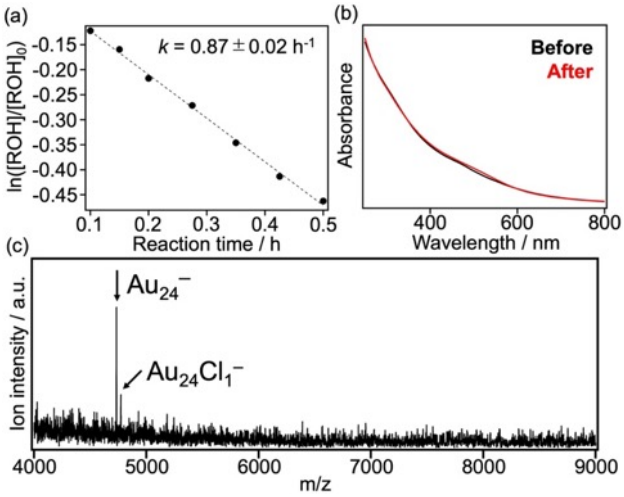

Figure S9. (a) Time course of substrate concentration in the catalytic oxidation of benzyl alcohol at 303 K. (b) Optical absorption and (c) MALDI mass spectra of Au_{24}:PVP after the catalysis.

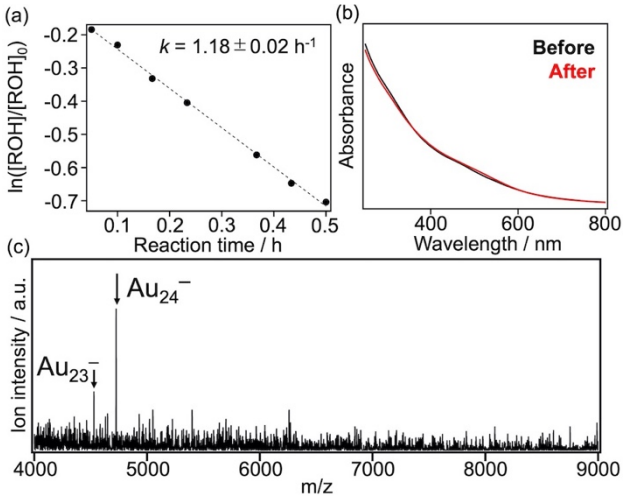

Figure S10. (a) Time course of substrate concentration in the catalytic oxidation of benzyl alcohol at 303 K under 1 atm of O_2. (b) Optical absorption and (c) MALDI mass spectra of Au_{24}:PVP after the catalysis.

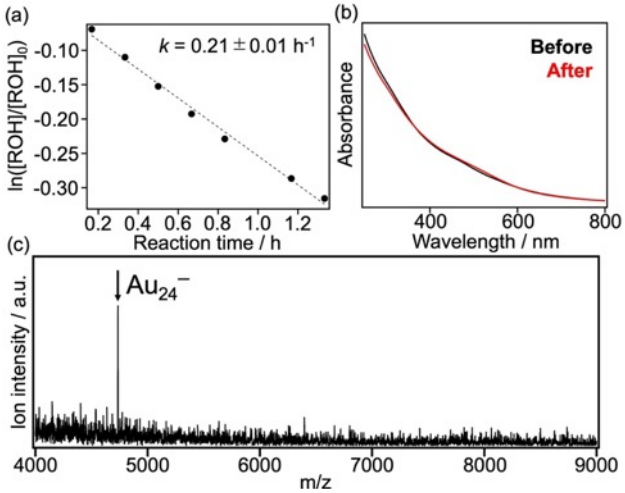

Figure S11. (a) Time course of substrate concentration in the catalytic oxidation of deuterated benzyl alcohol ($C_6H_5CD_2OH$) at 303 K. (b) Optical absorption and (c) MALDI mass spectra of Au_{24}:PVP after the catalysis.

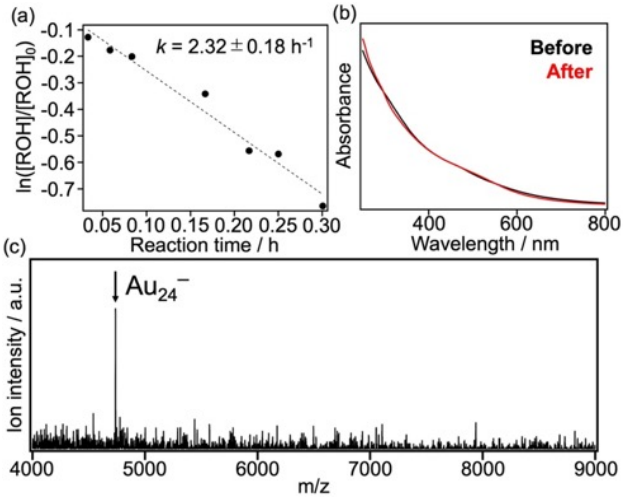

Figure S12. (a) Time course of substrate concentration in the catalytic oxidation of *p*-methoxybenzyl alcohol ($CH_3OC_6H_4CH_2OH$) at 303 K. (b) Optical absorption and (c) MALDI mass spectra of Au_{24}:PVP after the catalysis.

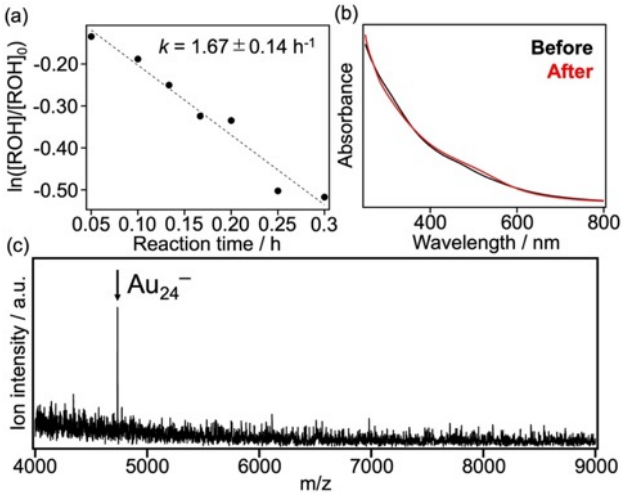

Figure S13. (a) Time course of substrate concentration in the catalytic oxidation of *p*-methylbenzyl alcohol ($CH_3C_6H_4CH_2OH$) at 303 K. (b) Optical absorption and (c) MALDI mass spectra of Au_{24}:PVP after the catalysis.

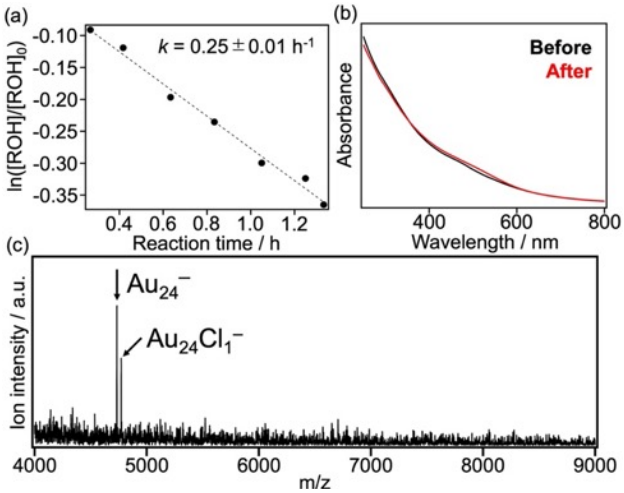

Figure S14. (a) Time course of substrate concentration in the catalytic oxidation of *p*-(trifluoromethyl)benzyl alcohol ($CF_3C_6H_4CH_2OH$) at 303 K. (b) Optical absorption and (c) MALDI mass spectra of Au_{24}:PVP after the catalysis.

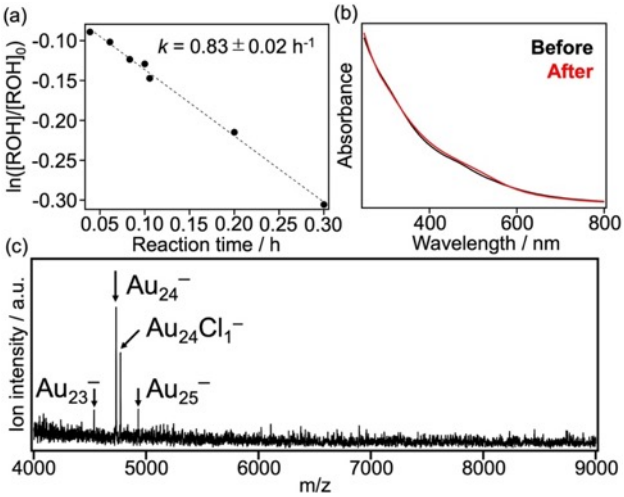

Figure S15. (a) Time course of substrate concentration in the catalytic oxidation of benzyl alcohol at 303 K. Although the batch of Au_{24}:PVP used for O_2 pressure dependence, the KIE, and Hammett plot (batch a, **Fig. S9**–**S14**) is different from that for the Arrhenius plot (batch b, **Fig. S15**–**S18**), the observed catalytic

activities of the two batches agreed well with each other (**Fig. S9** and **S15**). (b) Optical absorption and (c) MALDI mass spectra of Au_{24}:PVP after the catalysis.

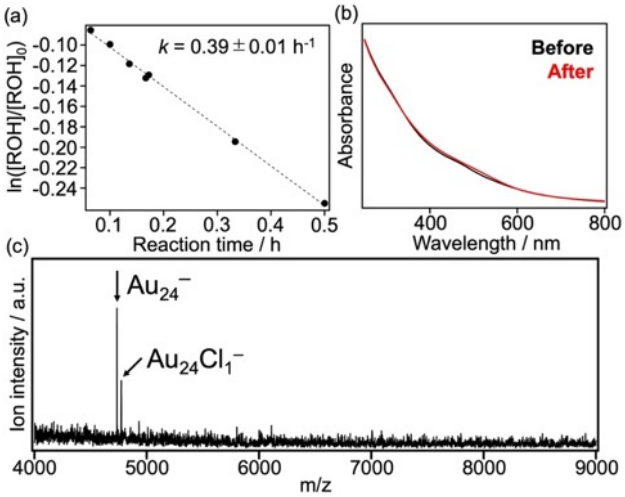

Figure S16. (a) Time course of substrate concentration in the catalytic oxidation of benzyl alcohol at 293 K. (b) Optical absorption and (c) MALDI mass spectra of Au_{24}:PVP after the catalysis.

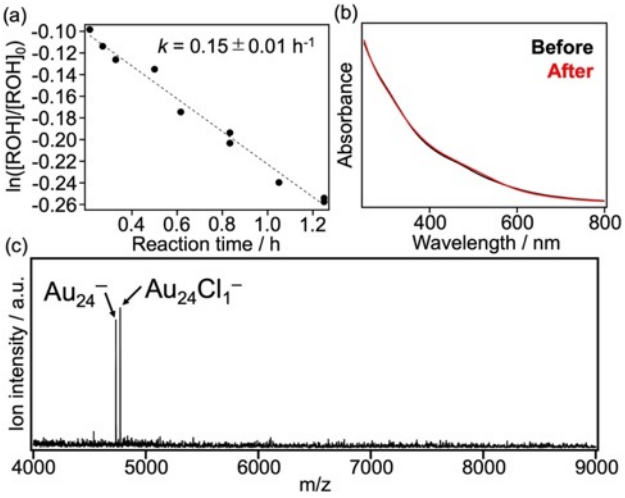

Figure S17. (a) Time course of substrate concentration in the catalytic oxidation of benzyl alcohol at 283 K. (b) Optical absorption and (c) MALDI mass spectra of Au_{24}:PVP after the catalysis.

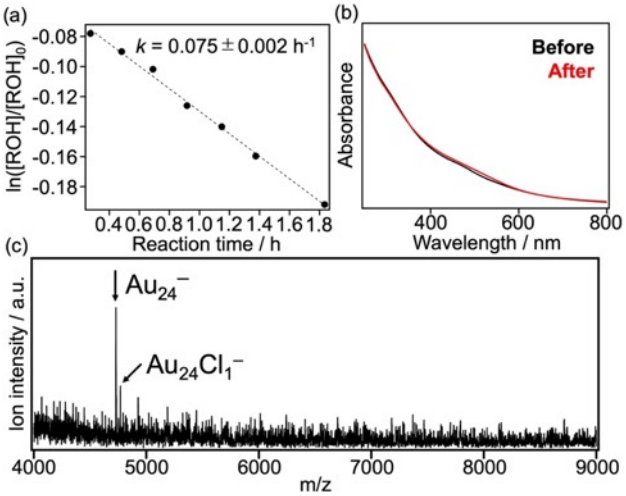

Figure S18. (a) Time course of substrate concentration in the catalytic oxidation of benzyl alcohol at 273 K. (b) Optical absorption and (c) MALDI mass spectra of Au_{24}:PVP after the catalysis.

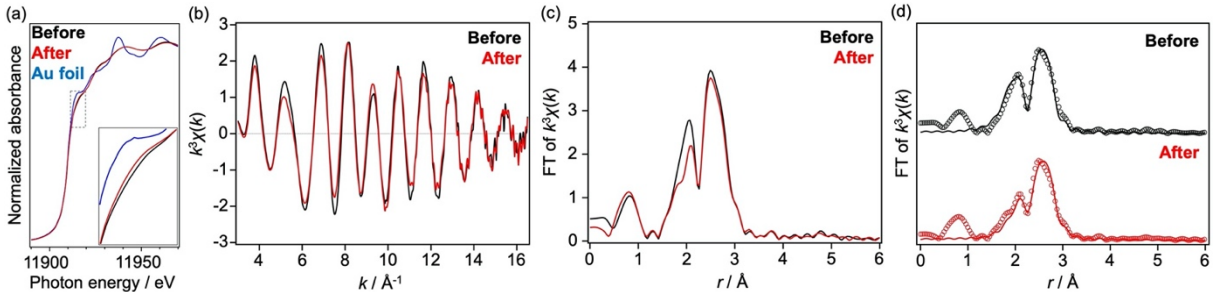

Figure S19. Au L_3-edge (a) XANES, (b) EXAFS, and (c) FT-EXAFS spectra of Au_{24}:PVP before (black) and after (red) the catalytic reaction under the same conditions as in **Figure S9** (benzyl alcohol oxidation at 303 K for 30 min). XANES spectrum of Au foil (blue) is also shown in (a) as a reference. (d) Comparison of the experimental (circles) and fitting (solid curve) FT-EXAFS spectra. The FT-EXAFS spectrum before the reaction is identical to that in **Figure 2c**.